Phys. Med. Biol. 38 (1993) 1545–1560. Printed in the UK

The spatial distribution of cavitation induced acoustic emission, sonoluminescence and cell lysis in the field of a shock wave lithotripter

A J Coleman†, M Whitlock†, T Leighton‡ and J E Saunders†
† Medical Physics Department, St Thomas' Hospital, London SE1 7EH, UK
‡ Fluid Dynamics and Acoustics Group, Institute of Sound and Vibration Research, Southampton SO9 5NH, UK

Received 29 March 1993, in final form 7 June 1993

Abstract. This study examines the spatial distribution of various properties attributed to the cavitation field generated by a shock wave lithotripter. These properties include acoustic emission and sonoluminescence, which result from violent bubble collapse, and the degree of cell lysis *in vitro*, which appears to be related to cavitation. The acoustic emission detected with a 1 MHz, 12 cm diameter focused hydrophone occurs in two distinct bursts. The immediate signal is emitted from a small region contained within the 4 MPa peak negative pressure contour. A second, delayed, burst is emitted from a region extending further along the beam axis. The delay between these two bursts has also been mapped, and the longest delay occurs at positions close to the regions of maximum peak negative pressure. Sonoluminescence from both single and multiple shocks occurs in a broader region than the acoustic emission but the measurement technique does not allow time resolution of the signal. Cell lysis occurs in a relatively small region that correlates closely with the immediate acoustic emission for a shock propagating in a gelatine solution.

1. Introduction

Acoustic cavitation plays a major role in extracorporeal shock wave lithotripsy. There is a range of studies demonstrating that cavitation contributes to stone fragmentation, and there is a growing literature on the biological effects of shock wave exposure on soft tissue and bone, in which transient cavitation is identified as the likely mechanism. These studies have recently been reviewed (Brummer *et al* 1990, Coleman and Saunders 1993).

In this study the spatial distributions of acoustic emission and sonoluminescence due to cavitation around the focus of an electrohydraulic lithotripsy source have been measured in water, along with the spatial distribution of the percentage of cell lysis resulting from the exposure of cells in suspension. The acoustic emission has also been examined in gelatine, at a concentration which is known to inhibit cell lysis. These distributions are compared with each other, and also with the measured distribution of temporal peak pressures in the shock wave field.

2. Methods

2.1. Experimental set-up

A laboratory electrohydraulic acoustic shock wave source has been used throughout this study (Coleman *et al* 1989). This device, operated at 21 kV, generates a focused

0031-9155/93/111545+16$07.50

field in water, similar to that of the clinical Dornier HM3 lithotripter. The source is aligned in a water tank so that the beam axis is horizontal. Hydrophones can be positioned in the underwater acoustic field using a three-axis stepper motor driven jig under computer control. Using a LeCroy 9450 digitizing scope and suitable hydrophones it is possible to store and analyse measured pressure waveforms on the computer. This set-up allows automated data collection at a large number of positions in the water tank, and display of a two-dimensional matrix of measurements as grey scale images or contour plots.

It has been noted in previous studies that electrohydraulic sources of the type used here emit several shock waves of decreasing amplitude at 3–4 ms intervals after a single firing (Coleman *et al* 1992). Data on the acoustic emission in water and gelatine has been obtained for the first two shocks, referred to here as primary and secondary shocks, to illustrate the effect of reduced amplitude on acoustic emission. Pressure measurements are presented for the primary shock field only. The secondary shock field has a similar spatial distribution, with absolute pressures less than 40% of the valuer for the primary shock. The images of sonoluminescence are obtained at exposure times longer than 4 ms and, as with the measured cell lysis, will be influenced by both primary and secondary shock wave induced cavitation.

2.2. *Pressure measurements*

The pressure field generated in tap water was mapped using a bi-laminar PVDF membrane hydrophone (Marconi Y-34-3598 IP116, with a 0.5 mm diameter sensitive element) connected to the 1 MΩ (15 pF) input of the oscilloscope via a −6 dB gain (50 Ω output) broadband amplifier (Marconi Y-34-6527 IP017). The sensitivity of this system was calculated from the National Physical Laboratory 1 MHz calibration of the hydrophone and amplifier to be 0.053 μV Pa^{-1}. Three repeated measurements of peak positive and negative voltage were obtained at positions separated by 10 mm intervals parallel to the beam axis, and at 5 mm intervals perpendicular to the beam axis in a vertical plane. Repeated measurements were not averaged but were placed in adjacent columns of a two-dimensional matrix (70 × 110 mm) which was then displayed as a contour plot. The region examined is illustrated in relation to the ellipsoidal reflector of the shock wave source and its geometrical focus (F2) in a scale drawing in figure 1.

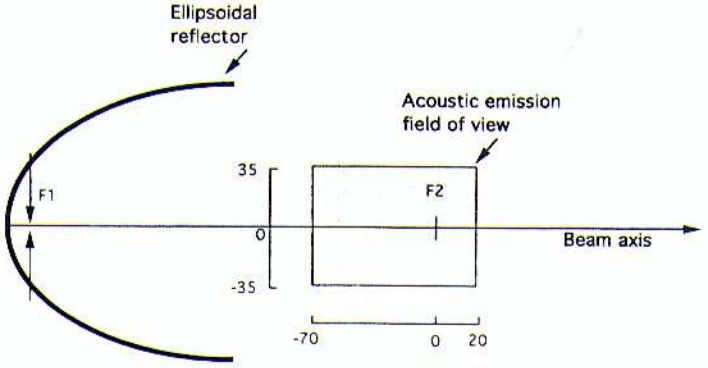

Figure 1. A scale diagram of the electrohydraulic shock wave source showing the position of the geometrical focus (F2) and the dimensions (in mm) of the region in which pressure and cavitation measurements have been made.

2.3. *Acoustic emission*

The acoustic emission from tap water at 20 °C following the passage of the shock wave has been measured using a 100 mm diameter 1 MHz PZT4 air-backed focused hydrophone (focal length 120 mm) in an identical manner to that described by Coleman *et al* (1992). The nominal sensitivity of this hydrophone, estimated from tabulated data, is 10 μV Pa^{-1}. Typically, the observed signal when the focus of this hydrophone is directed towards the focus of a shock wave source, as described by Coleman *et al* (1992), takes the form of an immediate burst of acoustic emission around the time of the shock wave arrival and a second burst delayed by a variable time of between 100 and 600 μs.

The amplitudes of the signals registered by the focused hydrophone due to the immediate and delayed bursts and the time between these are recorded at different positions as the beam focus of the hydrophone is scanned in discrete steps in a vertical plane containing the beam axis of the shock wave source (the field of view in figure 1). Three measurements of each parameter are made at each position within the field of view (70 × 90 mm^2). As for the pressure measurements, repeated measurements were not averaged but were placed in adjacent columns of a two-dimensional matrix of values (15 × 30) which was then displayed as a smoothed grey scale image or a contour plot. This procedure is designed to reflect the 'all or nothing' nature of the cavitation signal and ensures that any signal detected at one location during the course of three repeated shocks shows on the grey scale image. Delay time measurements were made from the oscilloscope trace, showing the immediate and delayed signals. For times more than about 150 μs such measurements could be made unequivocally with an accuracy of better than 10 μs by placing the oscilloscope time difference cursors on the two highest peaks in the trace. Delay times shorter than about 150 μs are found to correspond to significantly lower-amplitude emission and unequivocal identification of the immediate and delayed peaks in the oscilloscope trace becomes more difficult. In these cases the time delay is set to 100 μs for the purpose of obtaining reasonable contour plots.

In an attempt to understand the role of any translational bubble motion, the acoustic emission measurements were repeated in 3% gelatine with a measured viscosity (when set at room temperature) of more than 10 times that of water, although the homogeneity of setting of the gelatine could not be verified. A plastic container with large acoustic windows made from 50 μm Mylar on all four sides was filled with the 3% gelatine solution. The gelatine occupied a volume at least as large as that of the cylinder formed by the source aperture, with a length of twice the focal distance, so that it contained most of the acoustic field. The focused hydrophone was scanned in an identical manner to that in water over the same field of view.

2.4. *Sonoluminescence*

Sonoluminescence from a horizontal plane containing the beam axis of the shock wave source was detected using a lens system located directly above the water tank, which focuses light onto the input phosphor of an (EMI type 9912) image intensifier. The output phosphor of this device is viewed using a video camera (Hamamatsu C-1000) attached to a recorder (JVC u-matic) and black and white monitor (Panasonic WV5360). The video image was then photographed. Further details of this system are given by Leighton *et al* (1988). The field of view of this system is considerably larger than that examined for the acoustic emission (figure 1) and contains the source aperture as well as the beam focus (F2).

2.5. Cell lysis

Radiation induced fibrosarcoma (RIF) cells were suspended in serum free growth medium at a concentration of 1×10^6 cells ml^{-1}. The cell suspension was transferred to the cylindrical bulb (length, 25 mm; diameter, 10 mm) of polyethylene miniliquipettes (Labsystems, UK) making sure that the neck of the pipette was filled to ensure that the air/liquid interface was at least 15 mm from the top of the bulb. Seven sealed bulbs were then placed in the water tank containing tap water at 20 °C. These were positioned in a row perpendicular to the shock wave axis so that each bulb was in contact with the adjacent bulbs. Ten such rows of bulbs were each exposed in turn to 200 shock waves (at 21 kV) with each row being placed at 10 mm intervals along the beam axis. The region of the shock wave field covered in this way extended from 70 mm in advance of the beam focus F2 to 20 mm beyond the focus, and extended 30 mm either side of the beam axis in the horizontal plane. Control samples were placed in the tank during exposure at a position well outside the acoustic shock wave field.

Following shock wave exposure the contents of each pipette were analysed on a FACScan flow cytometer (Becton Dickinson Inc., USA). Cells with damaged membranes were discriminated from intact cells by measuring the uptake of the fluorescent dye propidium iodide. Ten thousand cells from each sample were analysed, and the percentage of cells with grossly increased propidium iodide uptake recorded as a measure of cell lysis. Cell debris with dimensions considerably less than normal cell size was easily identified by the low-side scatter and excluded from the measurement.

3. Results

3.1. Pressure distribution

Contour plots of peak positive and negative pressures (in MPa) are shown in figure 2 (top and bottom panels, respectively). The spatial distribution of peak positive pressures (top panel) has its maximum (of 47 MPa) 20 mm beyond the geometrical focus of the source (F2). Smaller spatial peaks containing maximum pressures of less than 40 MPa appear at a positions 30 mm beyond and 10 mm in front of F2. In contrast, the spatial distribution of peak negative pressure (bottom panel) shows a single spatial maximum (of 10 MPa) at a position 26 mm before F2.

The appearance of three peaks (top panel) is an artifact of the measurement and display procedure, in which each of the three recorded values of pressure are placed in adjacent columns of a matrix of values before interpolation to find the contours. The shock to shock variation in peak positive pressure at any one position in the acoustic field is about 25% and individual high readings, therefore, appear in the contour plot as separate peaks. This procedure, which avoids averaging recorded pressures, is used to be consistent with that used in displaying the 'all or nothing' signal from cavitation. While a plot of averaged values would contain a single peak of around 30 MPa about 5 mm beyond F2 (Coleman and Saunders 1990), the contours in the top panel of figure 2 have the advantage of illustrating the true recorded pressures, and the fact that high positive peak pressures can be reached intermittently either side of F2.

The differential focusing of negative and positive peak pressures shown in figure 2 is a consequence of the non-linear nature of the field and is expected from diffraction considerations (Choi 1992). For this study, the separation of the positive and negative

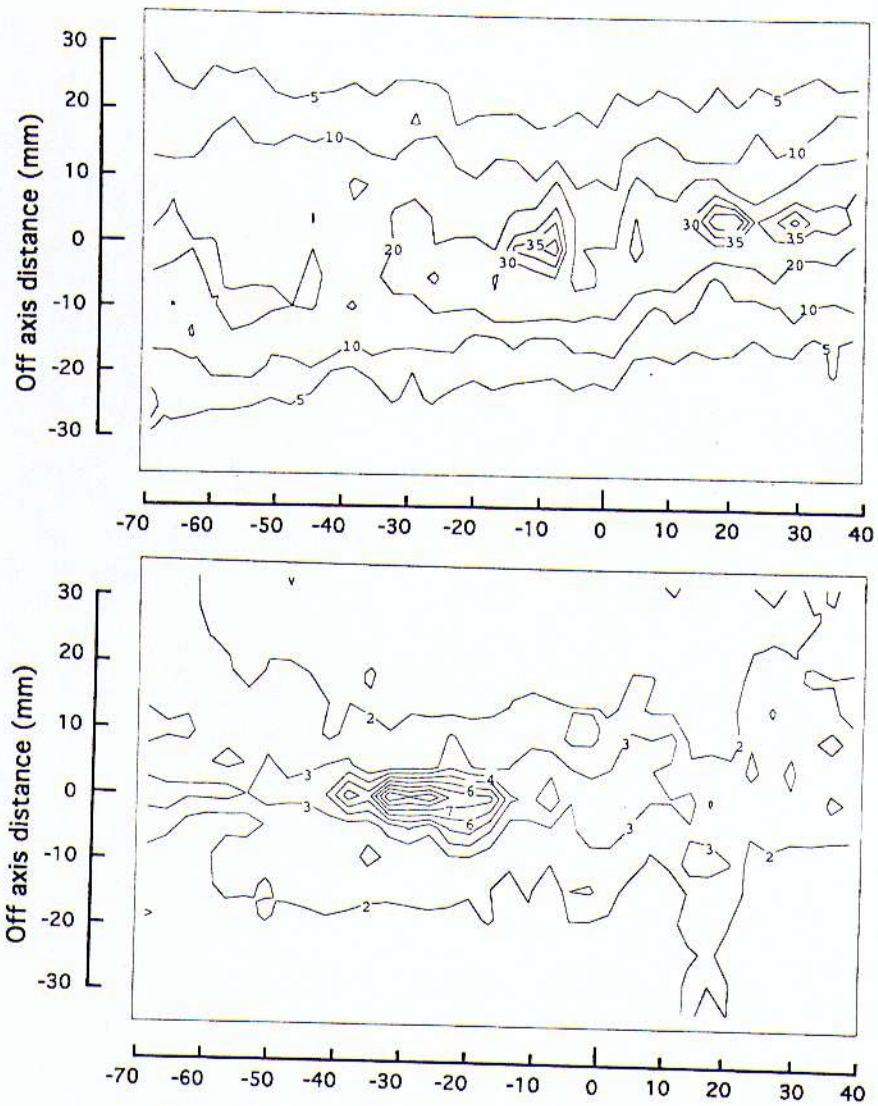

Figure 2. A contour plot of the temporal peak positive (top panel) and peak negative (bottom panel) pressures (in MPa) in a region around the beam focus. Vertical and horizontal scales are in millimetres, measured from the geometrical focus (F2).

peak pressure foci is useful since the influence of these parameters on the cavitation field can, to some extent, be separately identified.

3.2. Acoustic emission in water

3.2.1. Primary shock. Figure 3 presents data obtained on the acoustic emission from the cavitation in water following the primary shock wave. The top panel is a grey scale image corresponding to the detected amplitude of the immediate signal (within 30 μs of the shock wave) within the region defined in figure 1. The middle panel represents the amplitude of the delayed signal in the same region. The bottom panel is a contour

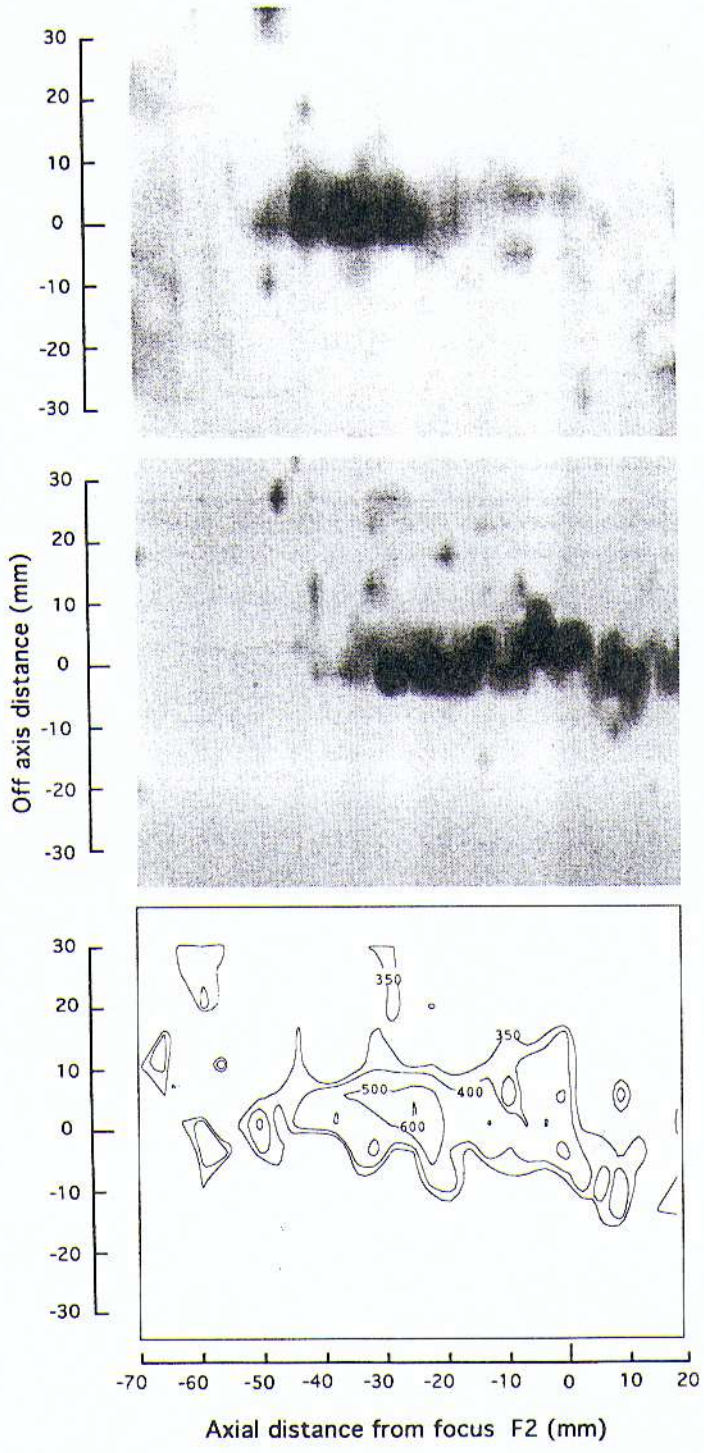

Figure 3. Grey scale images of the amplitude of the acoustic emission in water induced by the primary shock from the immediate signal (top panel) and the delayed signal (middle panel). A contour plot of the time between immediate and delayed signals (in μs) is given in the bottom panel.

map of the measured time period (in μs) between the immediate and delayed acoustic emission signals.

It is evident from the grey scale images in figure 3 that the immediate signal is contained within a small region centred about 30 mm before F2 and that the delayed signal appears to emerge from a region more widely spread along the beam axis which extends beyond F2. If it is assumed that the enlargement of the emission region can be considered to result from bubble movement between the recording of the immediate and delayed signals then it is apparent from figure 3 that a 30 mm movement occurs in about 400 μs, corresponding to an average bubble velocity of about 75 m s^{-1} in the direction of shock propagation.

The average immediate emission amplitude is about 85% of that due to the delayed signal (maximum 460 mV) and in both cases the background level off axis is about 80 mV. The maximum delay time (600 μs) occurs at the same position as the maximum amplitude of the immediate signal. The noise level in these measurements, obtained from the oscilloscope trace before the shock wave arrival, is less than 5 mV.

3.2.2. Secondary shock. Grey scale images corresponding to the amplitude of the immediate and delayed acoustic emission in response to the secondary shock wave are shown in figure 4 (top and middle panels respectively) along with a contour map of the corresponding delay time (bottom panel). The data for these images were obtained from the same oscilloscope traces as used to acquire the amplitudes and delay times resulting from the primary shock used in figure 3. The peaks on the oscilloscope trace associated with the secondary shock occur, however, some 4 ms later and are, therefore, easily distinguished from those associated with the primary shock.

The maximum signal amplitude for both immediate and delayed emission induced by the secondary shock is 50% of that due the primary shock. The immediate signal (figure 4, top panel) arises from a larger region than that for the primary shock (figure 3, top panel). As for the primary shock, the delayed signal has a higher amplitude than the immediate signal, in this case, almost double. Comparison of the delay time contours (figure 4, bottom panel) with the corresponding set for the primary shock (figure 3, bottom panel) show that the delay time is about 50% shorter at all positions at which acoustic emission could be detected.

It is interesting to note that the acoustic emission resulting from the secondary shock (figure 4, top and middle panels) appears from a region parallel to but about 5 mm below the beam axis. In the primary pulse, emission is centred about the beam axis. This difference implies that the bubbles have drifted down in the water, or that the shock wave field has shifted, during the 4 ms interval between primary and secondary shocks.

3.3. Acoustic emission in gelatine

3.3.1. Primary shock. Acoustic emission data for the primary shock in gelatine are presented in figure 5. The maximum amplitudes of the immediate and delayed signals (top and middle panels, respectively) are lower than those recorded in water; the maximum immediate signal amplitude is 55% of that in water and the delayed signal about 76%. Both immediate (top panel) and delayed (middle panel) emission in gelatine appear from regions before F2, as in water, but in both cases emission commences at a position some 10 mm closer to F2 than in water. The delay times (bottom panel) are less than those produced in water by the primary shock (figure 3).

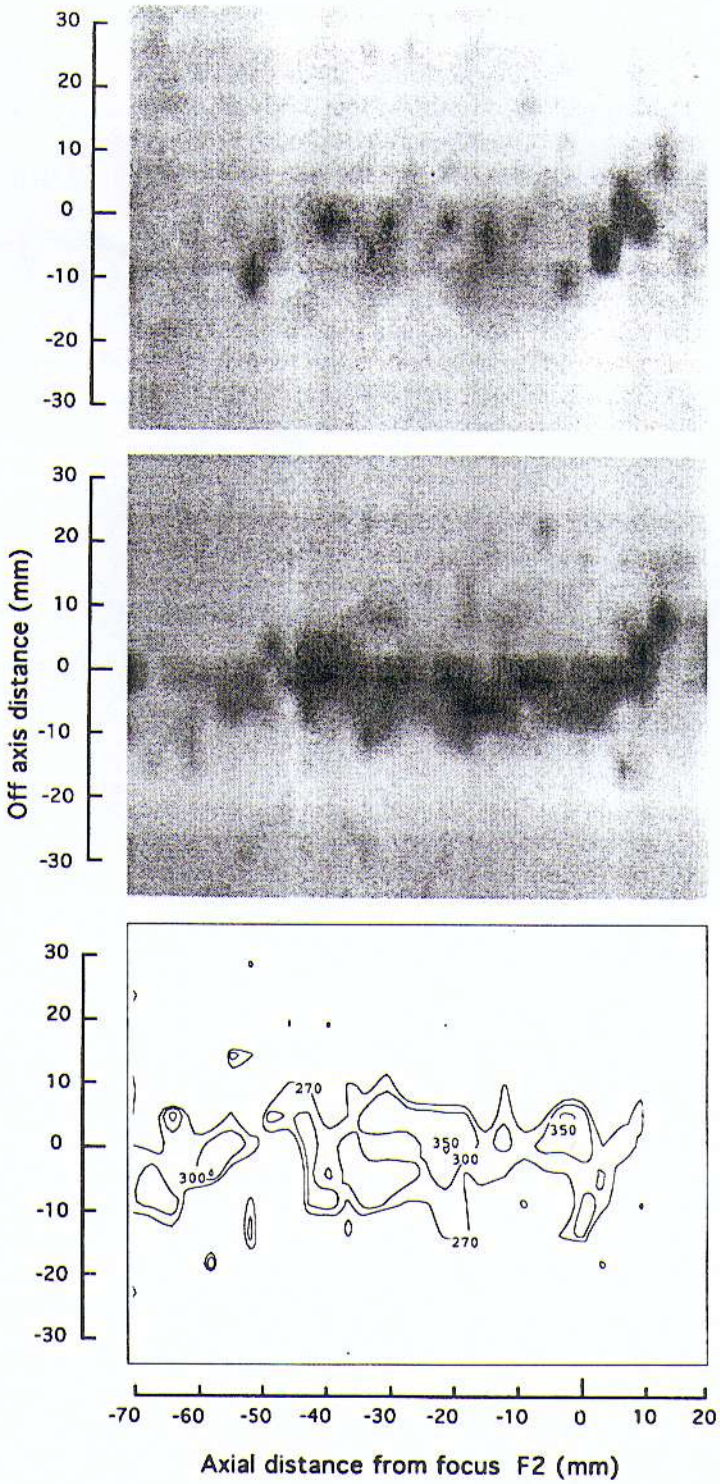

Figure 4. Grey scale images of the amplitude of the acoustic emission in water induced by the secondary shock from the immediate signal (top panel) and the delayed signal (middle panel). A contour plot of the time between immediate and delayed signals (in μs) is given in the bottom panel.

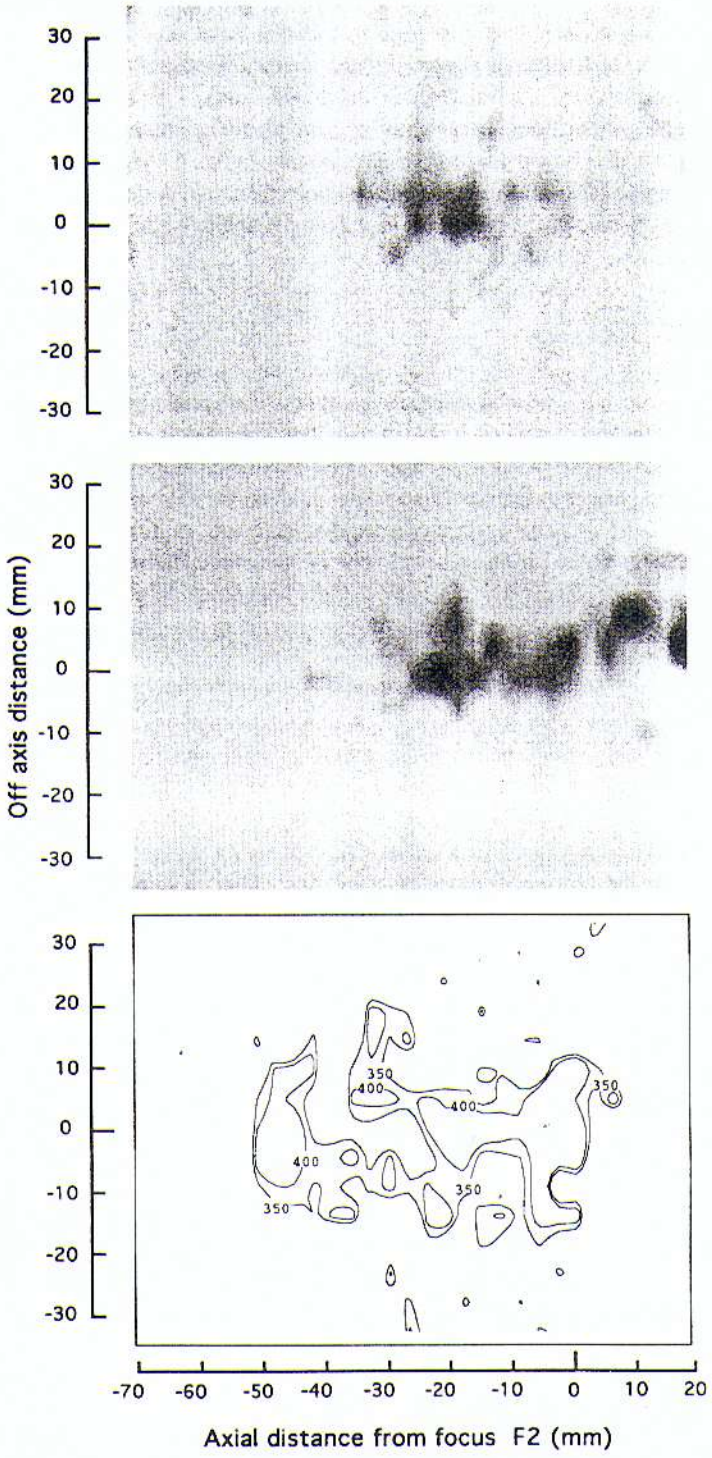

Figure 5. Grey scale images of the amplitude of the acoustic emission in 3% gelatine induced by the primary shock from the immediate signal (top panel) and the delayed signal (middle panel). A contour plot of the time between immediate and delayed signals (in μs) is given in the bottom panel.

3.3.2. Secondary shock. Immediate and delayed acoustic emission resulting from the secondary shock (figure 6, top and middle panels) have, as expected, lower amplitudes than those from the primary shock (figure 5). In this case, the maximum immediate signal amplitude is 50% of that of the delayed signal. The spatial distribution of the immediate signal is confined to a small region about 20 mm before F2, in contrast to the broad region extending beyond F2 in water (figure 4, top panel). Both immediate and delayed signals (top and middle panels) commence at a position some 20 mm closer to F2 than the corresponding signals in water (figure 4, middle panel). Delay times are about 50% of those in the primary shock in gelatine.

3.4. Sonoluminescence

Images of sonoluminescence from an identical shock wave source operated at 20 kV are shown for the case of a single firing (figure 7(a)) and for 10 repeated firings at a nominal pulse repetition rate of 1 Hz (figure 7(b)). The large bar to the left of each figure represents the source aperture (154 mm). The rectangular box enclosing the focus (F2) in figure 7 represents the dimensions of the field of view used in the acoustic emission measurements, and is shown to facilitate comparison of the images. Figure 7(b) was obtained from the video image photographed with the camera shutter left open until after the last shock (i.e. a 10 s exposure time). The level of photon and ion spot noise in the image intensifier can be estimated from the spots that occur in the images at positions behind the aperture.

The spatial distribution of sonoluminescence obtained with a single shock (figure 7(a)) is considerably narrower than that obtained with 10 shocks, and most of the detected sonoluminescence from a single shock occurs, in contrast to that from multiple shocks, before F2. Such differences are consistent with the assumption that bubbles generated by a single shock may subsequently move along and away from the beam axis over the course of 10 shocks.

It is difficult to compare these sonoluminescence images with those of acoustic emission, since they do not allow resolution of any time variation in the signal. The single-shot image of sonoluminescence (figure 7(a)) does show a distribution not dissimilar to that of delayed acoustic emission in water (figure 3, middle panel) for events close to the beam axis within the same field of view. However, the presence of sonoluminescence signal at distances more than twice the focal length from the aperture suggests that significant translational movement has occurred during the exposure time (of more than 1 s) if, as seems likely, it is assumed that the shock wave field is too weak to activate bubbles at this distance.

3.5. Cell lysis

Contours of the percentage cell lysis are plotted in figure 8. To provide some comparison with a physical measurement of the cavitation field the lysis contours are superimposed on the grey scale image of the immediate acoustic emission amplitude from cavitation induced by the primary shock wave propagating in gelatine (figure 5, top panel). This image is chosen since it appears to correlate best with the cell lysis contours. It is interesting to note that the peak cell lysis (7%), and immediate acoustic emission in gelatine, occur about 20 mm in front of F2 compared with 30 mm for the maximum peak negative pressure (figure 2, lower panel) and immediate acoustic emission in water (figure 3, top panel).

The reason for any correlation between cell lysis and immediate acoustic emission

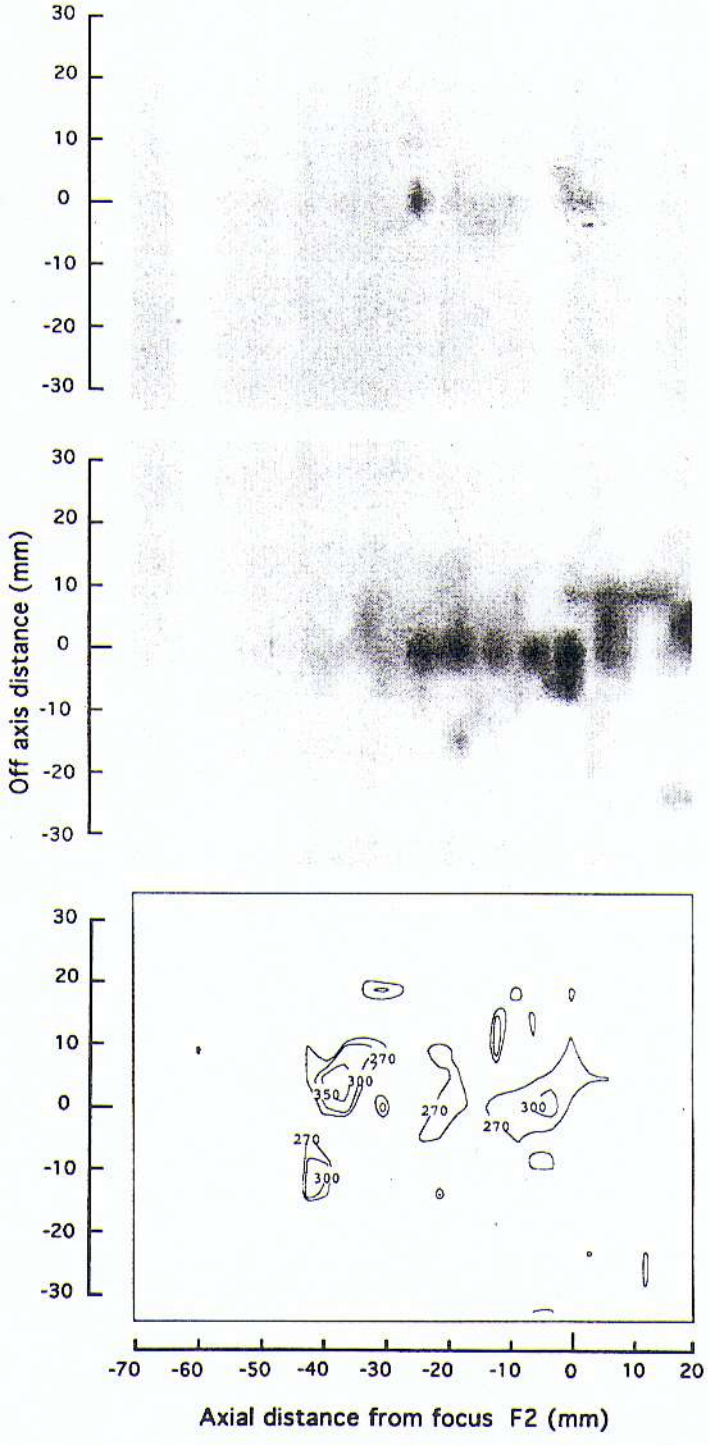

Figure 6. Grey scale images of the amplitude of the acoustic emission in 3% gelatine induced by the secondary shock from the immediate signal (top panel) and the delayed signal (middle panel). A contour plot of the time between immediate and delayed signals (in μs) is given in the bottom panel.

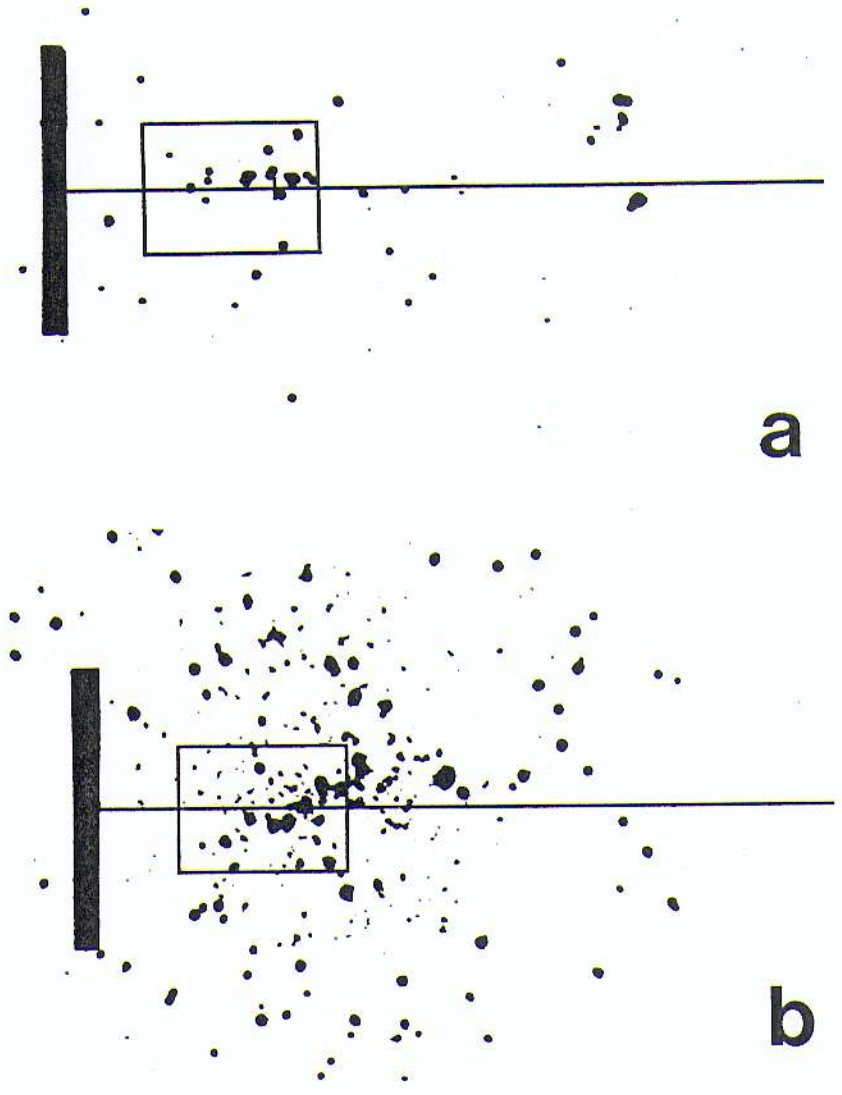

Figure 7. Images of the sonoluminescence resulting from (a) one discharge and (b) 10 discharges at 1 Hz in water recorded using an image intensifier system. The source aperture (of diameter 154 mm) is represented by a vertical bar on the left of the image and the field of view used in the acoustic emission measurements is contained in the box enclosing the geometrical focus F2.

from cavitation in gelatine, rather than water, is not clear. It is evident, however, that lysis of cells exposed in small pipettes cannot be influenced by bubbles originating outside the pipette and, for this reason, any effect of bubble movement over distances larger than 10 mm (the pipette diameter) will have no influence on any cavitation induced cell lysis in this experiment. It is possible to argue that the immediate acoustic emission would be expected to correlate with any cavitation induced lysis better than the delayed emission since immediate emission presumably occurs before appreciable translational bubble movement can take place.

The location of maximum cell lysis is, as already noted, about 10 mm closer to F2

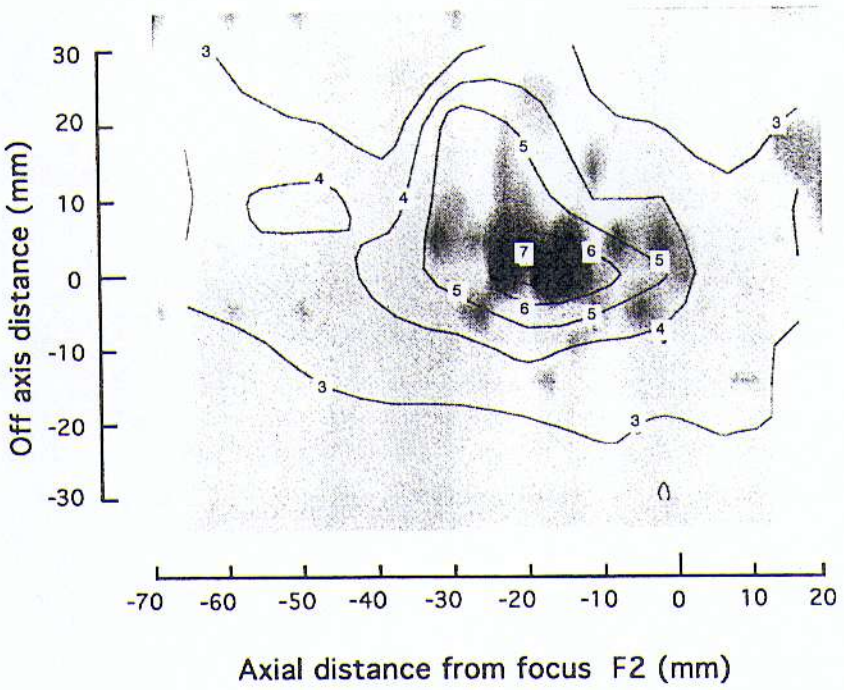

Figure 8. Contours of the percentage lysis of radiation induced fibrosarcoma (RIF) cells *in vitro* following 200 shocks. The contours are superimposed on the grey scale image of the delayed acoustic emission signal amplitude for the primary shock wave in 3% gelatine.

than the location of the peak negative pressure (figure 2, lower panel) and the immediate emission signal in water. This same shift is observed in the immediate acoustic emission from gelatine, and may be a result of attenuation of the shock wave field. Attenuation by gelatine or the plastic of the pipette may be sufficient to reduce the size of the region within which the cavitation threshold is exceeded, and shift the position of cavitation onset towards F2.

4. Discussion

It has been demonstrated that the immediate acoustic emission in water and gelatine following exposure to a single lithotripter pulse originates from a relatively small well defined region. In water this region coincides with the position of high temporal peak negative pressure. While such a close correlation between negative pressures and cavitation may be expected from theoretical considerations, such a correlation has not previously been demonstrated experimentally in lithotripsy fields.

This correlation is illustrated in figure 9, which shows a grey scale image of the immediate acoustic emission in tap water with isobars of peak negative pressure superimposed. Most of the detected emission occurs within the 4 MPa isobar. By selecting out the immediate from the delayed emission the cavitation detection technique used here appears to allow bubble activity to be detected before translational bubble motion broadens this region. Similar comparisons of images of immediate acoustic

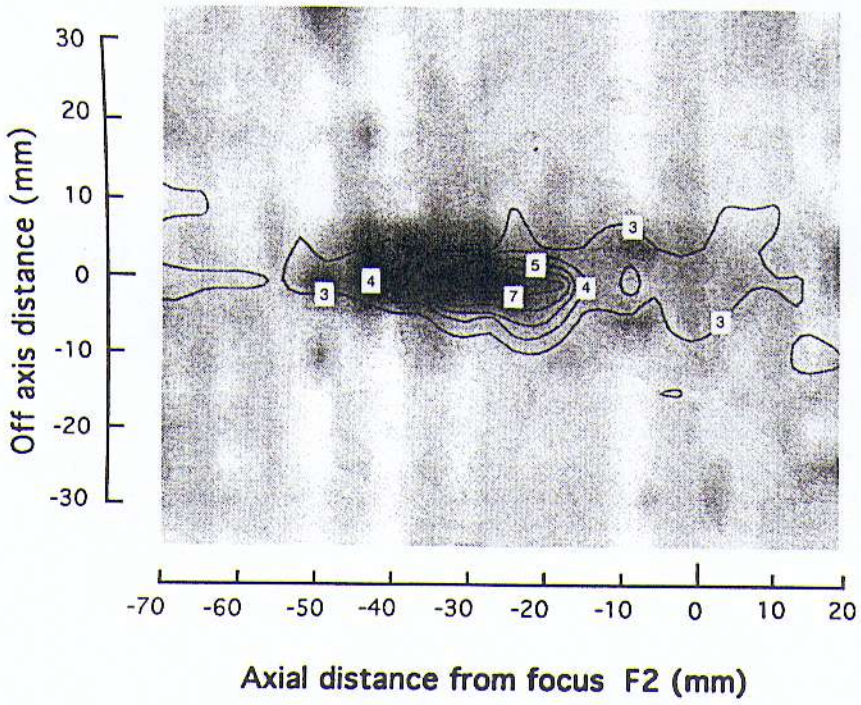

Figure 9. Temporal peak negative pressure contours measured in water, superimposed on the grey scale image of the amplitude (in MPa) of the immediate acoustic emission signal for the primary shock wave in water.

emission with contours of negative pressures may prove useful in determining cavitation thresholds in tissue using clinical lithotripsy to probe for cavitation nuclei.

The images of sonoluminescence presented here show evidence of relatively slow acoustic streaming away from the beam axis, with bubbles being dispersed widely throughout the acoustic field after multiple shocks. Vortices capable of dispersing bubbles in this way will, presumably, be set up as a result of interactions between the observed rapid streaming near the beam axis with the slower-moving or stationary fluid at off-axis positions. The sonoluminescence images are not directly comparable to those of acoustic emission since they represent time averaged properties of the cavitation field.

Rapid translational bubble motion is restricted to 10 mm inside the plastic pipettes used to hold the cell suspension in the shock wave field. Not surprisingly, therefore, cell lysis is not widely distributed in the field as suggested by the sonoluminescence images, but is confined to a region which is well in advance of the geometrical focus (F2) and similar to that from which immediate acoustic emission is observed in gelatine. The mechanism of the cell lysis, however, remains unclear and could be related to shear stresses induced as a result of either rapid translational or radial bubble motion. While cell lysis is known to be inhibited when cells are suspended in 3% gelatine, the evidence here suggests that neither radial nor translational bubble motions appear to be greatly reduced in this medium.

Accurate measurement of the delay time between emissions at different positions in the field has been shown to be possible. It is also shown that reduced shock amplitude resulting either from a lower-amplitude secondary shock or from attenuation of the primary shock in an attenuating medium (such as gelatine) results in smaller time delays,

as predicted theoretically. Moreover, the delay time contours correspond more closely to those of the peak negative pressure distribution than those of the positive pressure distribution, as predicted theoretically (Choi *et al* 1993, Church 1989) confirming that these delay times may, indeed, provide a means of estimating *in situ* negative pressures.

There are two clear discrepancies between the measurements presented here and the theoretical predictions of acoustic emission expected in response to a lithotripsy pulse (Choi *et al* 1993) which need further study. Firstly, as highlighted here, the immediate acoustic emission occurs in a region bounded by the negative pressure contours. This is contrary to the theoretical prediction that the first bubble collapse should not be influenced by negative pressures and should, instead, be closely associated with the region of maximum positive pressure. One possible explanation is that the immediate acoustic signal does not result from the bubble collapse, but rather from scattering of the edge waves into the focused hydrophone by enlarged bubbles. This model would also explain the relatively large magnitude of this signal, which, in theory, should be two orders of magnitude lower than that of the delayed signal. However, evidence that sonoluminescence detected using a photomultiplier tube occurs in both immediate and delayed bursts in the same way as the acoustic emission (Coleman *et al* 1992) suggests that there is, as predicted, a strong immediate collapse. A useful study would be to map the immediate and delayed sonoluminescence signal amplitude to clarify this point.

Secondly, the translational motion of the bubble appears to be an order of magnitude higher than the value of 4 m s^{-1} (Church 1989) predicted from consideration of the radiation force on the bubble and the viscous drag in water. As already noted, the higher viscosity of gelatine appears, experimentally, to have had no effect on translational motion. This casts some doubt on the assumption that the apparent spreading of the region of acoustic emission results from translational bubble motion. Rapid bubble motion can, however, be identified in ultrasound images of water at the focus of lithotripters. Further experiments made in homogeneous high-viscosity fluids should be able to clarify this point.

5. Conclusions

One of the most promising aspects of this line of work is its potential in determining cavitation thresholds in tissue. This application is suggested principally because the high-amplitude fields used in lithotripsy clearly generate acoustic emission from bubbles of a sufficient amplitude to suggest that this emission may be detectable in tissue. In addition, these are the only routinely used medical ultrasound fields in which relatively violent cavitation is probably essential in producing the therapeutic effect. If the collapse delay timing can, indeed, be related to negative pressure, as suggested here, then careful study of the acoustic emission from cavitation during clinical lithotripsy might provide valuable information on the negative pressures at which collapse cavitation occurs in human tissues.

Acknowledgments

We are grateful to Dr M J Choi for useful discussions on the interpretation of the data and to the Radiation Physics Workshop at St Thomas' Hospital for their assistance with the hydrophone positioning system. This work was supported partly by an MRC project grant (No G9028377SA).

References

Brummer F, Brauner Th and Hulser D F 1990 Biological effects of shock waves *World J. Urol.* **8** 224–32

Choi M J 1992 Theoretical aspects of high amplitude pulsed ultrasound used in lithotripsy *PhD Thesis* University of Bath

Choi M J, Coleman A J and Saunders J E 1993 The influence of fluid properties and pulse amplitude on bubble dynamics in the field of a shock wave lithotripter *Phys. Med. Biol.* **38** 1561–73

Church C C 1989 A theoretical study of cavitation generated by an extracorporeal shock wave lithotripter *J. Acoust. Soc. Am.* **86** 215–227

Coleman A J, Choi M J, Saunders J E and Leighton T G 1992 Acoustic emission and sonoluminescence due to cavitation at the beam focus of an electrohydraulic shock wave lithotripter *Ultrasound Med. Biol* **38** 1561–73. **18** 267–281

Coleman A J and Saunders J E 1990 A comparison of PVdF hydrophone measurements in the acoustic field of a shock wave source *Extra- und Intrakorporale Lithotripsie* ed Ch Ell, M Marberger and P Berlien (Stuttgart: Thieme) pp 14–22

—— 1993 A review of the physical properties and biological effects of the high amplitude acoustic fields used in extracorporeal lithotripsy *Ultrasonics* **31** 75–89

Coleman A J, Saunders J E and Choi M J 1989 An experimental shock wave generator for lithotripsy studies *Phys. Med. Biol.* **34** 1733–1742

Leighton T G, Pickworth M J W, Walton and Dendy P P 1988 Studies of the cavitational effects of clinical ultrasound by sonoluminescence: 1. Correlation of sonoluminescence with the standing wave pattern in an acoustic field produced by a therapeutic unit *Phys. Med. Biol.* **33** 1239–1248